The Size Distribution of Near-Earth Objects Larger Than 10 m

D. E. Trilling[1,2,3,8] , F. Valdes[4] , L. Allen[4,8] , D. James[5,8] , C. Fuentes[6,8], D. Herrera[4,8], T. Axelrod[7,8] , and J. Rajagopal[4,8]

[1] Department of Physics and Astronomy P.O. Box 6010 Northern Arizona University Flagstaff, AZ 86011, USA; david.trilling@nau.edu
[2] South African Astronomical Observatory P.O. Box 9 7935 Observatory, South Africa
[3] University of the Western Cape Bellville Cape Town 7535, South Africa
[4] National Optical Astronomy Observatory 950 N. Cherry Avenue Tucson, AZ 85719, USA
[5] Cerro Tololo Inter-American Observatory National Optical Astronomy Observatory Casilla 603 La Serena, Chile
[6] Departamento de Astronomia Universidad de Chile Camino El Observatorio #1515 Casilla 36-D Las Condes Santiago, Chile
[7] University of Arizona Steward Observatory 933 N. Cherry Avenue Tucson, AZ 85721, USA

Abstract

We analyzed data from the first year of a survey for Near-Earth Objects (NEOs) that we are carrying out with the Dark Energy Camera (DECam) on the 4 m Blanco telescope at the Cerro Tololo Inter-American Observatory. We implanted synthetic NEOs into the data stream to derive our nightly detection efficiency as a function of magnitude and rate of motion. Using these measured efficiencies and the solar system absolute magnitudes derived by the Minor Planet Center for the 1377 measurements of 235 unique NEOs detected, we directly derive, for the first time from a single observational data set, the NEO size distribution from 1 km down to 10 m. We find that there are $10^{6.6}$ NEOs larger than 10 m. This result implies a factor of 10 fewer small NEOs than some previous results, though our derived size distribution is in good agreement with several other estimates.

Key words: minor planets, asteroids: general – surveys

1. Introduction

Near-Earth Objects (NEOs) are minor solar system bodies whose orbits bring them close to the Earth's orbit. NEOs are important for both scientific investigations and planetary defense. Scientifically, NEOs, which have short dynamical lifetimes in near-Earth space, act as dynamical and compositional tracers from elsewhere in the solar system. Studying NEOs also has the practical application of searching for NEOs that could impact the Earth and potentially cause widespread destruction. Critically, the number of Chelyabinsk-sized bodies (10–20 m) is not well-constrained due to various assumptions made in calculating that population. This leads to significant uncertainty in the impact risk of these relatively common and relatively hazardous events.

Most NEOs are discovered by a small number of dedicated surveys, including the Catalina Sky Survey (Christensen et al. 2014), the Pan-STARRS survey (Wainscoat et al. 2014), and the restarted NEOWISE mission (Mainzer et al. 2014), and more than 1000 NEOs are discovered every year. The optical surveys (CSS, PS) use 1–2 m class telescopes, and their limiting magnitudes are roughly $V \sim 21$. The goal of these surveys is to discover as many NEOs as possible, so any aspect of the survey that diminishes discovery efficiency is eliminated.

We have carried out an NEO survey using the 3 deg^2 Dark Energy Camera (DECam; Depoy et al. 2008) with the 4 m Blanco telescope at the Cerro Tololo Inter-American Observatory (CTIO); for the purposes of moving object measurements, this combination of camera and telescope has been assigned the observatory code W84 by the Minor Planet Center. Our program was allocated 10 dark nights per "A" semester in 2014, 2015, and 2016, and is described in detail in L. Allen et al. (2017, in preparation). The etendue (product of aperture size and field of view) of this survey is a factor of 2–10 larger than that of other ground-based optical surveys, but our duty cycle of 10 nights per year is quite small in comparison to the typical 200 nights per year for dedicated surveys. The observational niche of our new observing program is therefore not in discovering a large number of NEOs, but rather (1) to discover faint NEOs, through our much larger aperture, and (2) to characterize our survey by implanting synthetic objects in our data stream, allowing us to debias and measure the size distribution of NEOs down to small sizes. The large-scale dedicated surveys (CSS, PS) cannot afford to detect and measure synthetic objects in their data stream, which increases processing time, but we can because of our comparatively short observing season. Of course, no synthetic objects are reported to the Minor Planet Center (MPC).

All NEO surveys are subject to observational incompleteness that results in detecting a biased sample. NEOs have a range of rates of motion, and because the flyby geometries vary, optical brightness does not necessarily correspond to NEO size. In order to measure the underlying size distribution of NEOs, knowledge of which NEOs are not detected is as important as knowledge of which NEOs are detected. The best way to measure this detection efficiency is through implanting synthetic NEOs—objects with the motions, PSFs, noise properties, etc., of real NEOs—into the data stream, and then detecting the fake NEOs in the same way as real NEOs are detected. Thus, the detection efficiency of the survey is readily measured as the number of synthetic NEOs detected over the number implanted as a function of magnitude (or rate of motion or orbital properties or any other aspect).

Here we combine our detected (real) NEOs with our measured detection efficiencies to derive, for the first time, the debiased size distribution of NEOs down to 10 m diameter as derived from a single telescopic survey. We find a factor of 10 fewer 10 m sized NEOs than extrapolations from larger sizes or normalization from terrestrial impact studies predict.

Some implications of this result are discussed at the end of this paper.

2. Observations and Data Processing

A detailed description of the observing cadence, sky coverage, filters, and exposure time is presented in L. Allen et al. (2017, in preparation). Here we use only results from our 10-night observing run in 2014 April/May. Briefly, each survey field ($3\,\mathrm{deg}^2$) was typically observed five times per night and on three nights. We observed using the broad VR filter.

The data processing steps are also presented in detail in Allen et al. In summary, each exposure is flat-fielded and astrometrically calibrated using the standard NOAO Community Pipeline (CP) for DECam (Valdes & Gruendl 2014). A photometric zeropoint, which leads to the reported magnitudes, is computed by matching stars to Pan-STARRS magnitudes (Magnier et al. 2013). However, in fields for which Pan-STARRS magnitudes were not available, the reference catalog used is the USNO-B1 photographic catalog (Monet et al. 2003) with a transformation designed to match, on average, the more accurate CCD magnitudes. For fields for which Pan-STARRS photometry is available, we transform the catalog g and r to V using a transformation[9] and then match the observed VR instrumental magnitudes to those values. For non-Pan-STARRS fields, we use USNO-B1 photographic magnitudes transformed to r (Monet et al. 2003), which gives us the pseudo-r magnitude. For the purposes of this paper, we treat all magnitudes that we reported to the MPC as V. We estimate that the photometric errors are typically less than 0.1 magnitudes, but formally use 0.2 mag here to include errors introduced by these various transformations. Our detection limit is around $\mathrm{SNR} \approx 5$ for objects that are not trailed or only slightly trailed; for trailed objects, our detection limit corresponds to $\mathrm{SNR} \approx 5$ per pixel at the brightest part of the trail.

A special version of the CP incorporating the NOAO Moving Object Detection System (Valdes 2015) adds the following steps. Exposures from each survey field in a night are median-combined to provide a reference image with transients removed. The median is subtracted from each contributing exposure to remove the static field. Catalogs of transient sources are created from the difference image. Objects with three or more detections with similar magnitudes that make a track of a consistent rate and with shapes (elongation/P.A.) consistent with that rate are identified as candidate moving objects. All objects with `digest2` scores[10] greater than 40% —that is, where the probability of being an NEO or other interesting object (Trojan, etc.), based on the short orbital arc, is greater than 40%—are verified through visual inspection to eliminate false detections (chance cosmic-ray alignments, etc.). All validated objects are submitted to the MPC; this list includes NEOs as well as many valid moving objects that are not NEOs.

Postage stamps of several representative NEOs observed by us are shown in Figure 1. A histogram of V magnitudes of our detected (real) NEOs is shown in Figure 2.

---

3. Detection Efficiency

One hundred synthetic NEOs, i.e., fake asteroids, are created in a square that circumscribes each pointing; on average, around 72 objects fall within the DECam field of view and not in gaps. These synthetic objects are implanted directly in each exposure. This is many more synthetic NEOs than real NEOs in each exposure, and allows us to probe the details of our sensitivity with a large number of objects. Over the entire observing run, around 365,000 synthetic asteroid detections were possible. The distributions of magnitude and rate of motion for the synthetic population are not matched to any specific underlying NEO population but do generally approximate an observed NEO population, while extending to much fainter magnitudes than could be detected in this survey (Figures 3 and 4). The synthetic objects are created independently for each field with simple linear motions; there is no linkage across fields or nights. The detected synthetic objects are identified based on their known implant positions. We recovered the synthetic asteroids in the same way as real asteroids, that is, satisfying the same minimum number (3) of observations per field, up to the point of running `digest2` (all synthetic objects would have high NEO probabilities), visual inspection (since these are known to be valid objects), and, naturally, reporting to the MPC. Postage stamp images of representative synthetic images are shown in Figure 1.

Two important features of the synthetic implants for the efficiency characterization are the seeing and streaking. The seeing of each exposure was used to provide a point-spread function (PSF) and the static magnitude of the source was trailed across the image based on its rate (as shown in Figure 1). These aspects affect the surface brightness, which means that the detection efficiency varies with the conditions on each night and field and the apparent rate of motion.

We note that our debiasing procedure requires the reasonable assumption that NEO sizes and albedos (in other words, their absolute magnitudes) are indepedent of flyby geometry (distance from the Earth, phase angle, etc.). Debiasing must only take into account the survey properties that bias our observed sample: magnitude and rate of motion, but not geometry. The measured detection efficiency as a function of magnitude is easily calculated as the number of synthetic NEOs detected divided by the number of synthentic NEOs implanted. The detection efficiency is calculated for each night and for each of four bins in the rate of motion (60–135, 135–210, 210–285, 285–360 arcsec hr^{-1}). Our measured detection efficiencies as a function of observed magnitude are shown in Figure 5. The overall detection efficiency for all synthetic objects as a function of H magnitude is shown in Figure 6.

For real objects, there are 303 unique "object-nights": a given object observed on a given night. As an example, 2014 HA$_{196}$ was discovered by us on 20140422 and reobserved by us on 20140427. This asteroid therefore has two "object-nights" and appears twice in our list of 303 "object-nights," giving us two different opportunities to debias the NEO population with this asteroid. Because we normalize our resulting size distribution (see below), counting individual objects more than once does not introduce a significant error for our result.
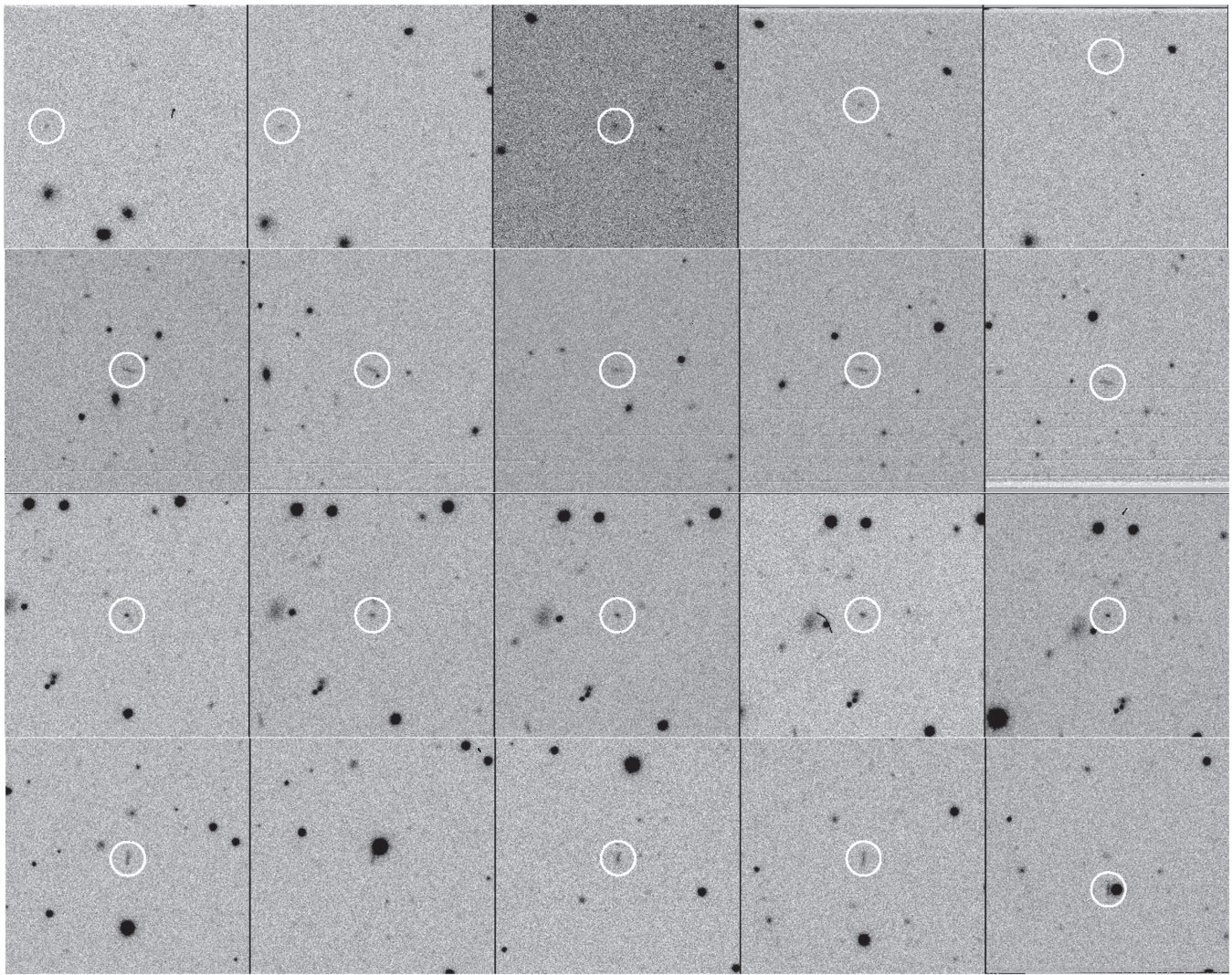
Figure 1. Postage stamps showing, from top to bottom, detections of real objects AiK41PR (rate of motion 138″/hr, magnitude 23.0) and AiNc1M6 (407″/hr, 22.3) and synthetic objects Sim_AiNd1U6 (98″/hr, 22.3), and Sim_AiNd1O1 (334″/hr, 21.3). From left to right in each row are the five images in our detection sequence, with typical time from the first to last image of around 20 minutes.
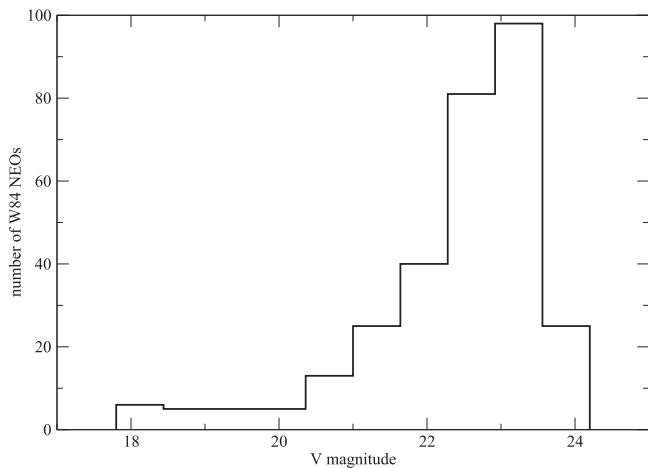
Figure 2. Histogram of transformed V magnitudes for all NEOs with preliminary or permanent designations that were detected in our DECam NEO survey (1377 observations of 235 objects). We show the first reported V magnitude for each object.
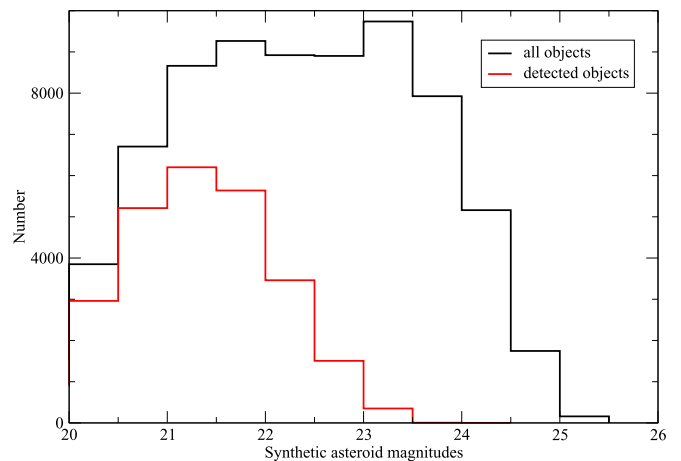
Figure 3. Magnitude distribution of synthetic (implanted) objects. The implanted population is not designed to mimic any particular underlying NEO population, but the overall shape is roughly similar to the expected distribution for a complete survey. The numbers shown on the vertical axis are in units of nightly tracklets, each of which consists in most cases of five observations, so, as an example, more than 50,000 individual NEO point sources were implanted with magnitudes in the range of 25–25.5.
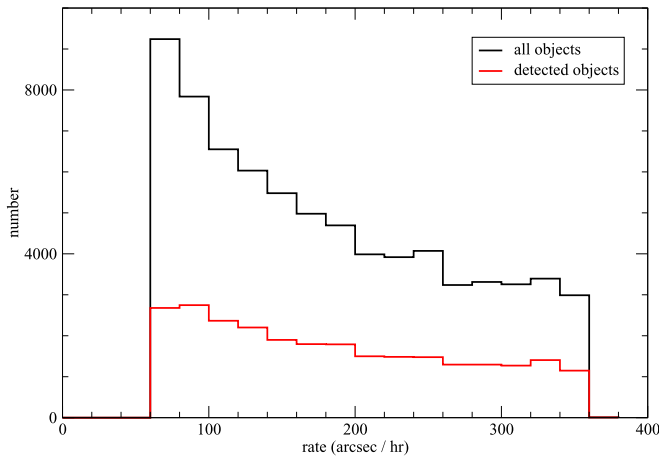
Figure 4. Rate distribution of synthetic (implanted) objects. The implanted population is not designed to mimic any particular underlying NEO population, but the overall shape is roughly similar to the expected distribution for a complete survey. We detected a handful of real NEOs with rates greater than the fastest synthetic NEO rate of 360 arcsec hr^{-1}. As in Figure 3, the numbers on the vertical axis are tracklets, not point-source images.

4. The Size Distribution of NEOs

Observations that meet the following criteria are used in this debiasing work: (1) the object observed must be classified as an NEO by the MPC; (2) the object observed has received either a preliminary designation (such as 2014 HD196, one of the W84 discoveries from the 2014 observing season) or permanent designation (for example, asteroid 88254, for which our nine W84 observations over two nights are only a small fraction of the more than 400 observations of this asteroid to date), which means that the orbit is relatively well known and therefore that both its NEO status and H magnitude are reasonably secure; and (3) the observations were made by us, i.e., observatory code W84. There are a total of 1377 measurements of 235 unique objects that meet these criteria. 97 of these objects were discovered by our survey.

When detected NEOs and the detection efficiency are both known, deriving the size distribution of NEOs is straightforward. Each ith NEO is detected at magnitude V_i and rate of motion r_i. The detection efficiency at that magnitude $\eta_i(V_i, r_i)$ is known (Figure 5). Each ith detected asteroid therefore, when debiased, represents $N_i = 1/\eta_i$ asteroids, applying the correction for the number of NEOs of that magnitude and rate of motion that exist but were not detected in our survey. Note that each NEO is debiased individually using the appropriate η for that object, using the nightly efficiencies shown in Figure 5.

The observed V magnitudes do not specify the size of the asteroid. The MPC processes the submitted astrometry to derive an orbit. Given that orbit and the reported magnitude, the solar system absolute magnitude H (the hypothetical magnitude an object would have at 1 au from the Sun, 1 au from the observer, and at zero phase) can be derived. For each ith asteroid, we use the MPC-derived absolute magnitude H_i. Figure 7 shows the histogram of all H magnitudes in our survey. Each ith asteroid therefore represents N_i asteroids with absolute magnitude H_i. Finally, we derive the cumulative size distribution $N(<H)$ by summing all N_i for a given $H \leqslant H_i$.

An asteroid's diameter D and H are related through the albedo p_V as

$$D = \frac{1329}{\sqrt{p_V}} 10^{-H/5} \qquad (1)$$

(Fowler & Chillemi 1992). We know nothing about the albedos of the NEOs we observed. Therefore, to calculate asteroid diameters, we adopt an albedo of 0.2, which is the average albedo from Mainzer et al. (2011) for bodies smaller than 200 m. We adopt this NEOWISE albedo value since their survey is relatively insensitive to asteroid albedo, unlike other NEO surveys; we discuss the uncertainties introduced by this assumption of a single average albedo below. There is therefore a direct translation from the absolute magnitude distribution to NEO size distribution. We calculate the cumulative size distribution: the number of objects larger than a given diameter.

The final step in deriving the size distribution of NEOs is a correction for the volume searched. This is analogous to the Malmquist bias present in flux-limited astrophysics surveys:[11] we can detect 100 m NEOs at a greater distance (and therefore in a greater volume) than we can detect 10 m NEOs. The NEO diameter D is given by

$$D \,(\mathrm{m}) = 2 \times \sqrt{\left(\frac{f_{\mathrm{NEO}}}{f_\odot}\right)\left(\frac{\Delta^2}{p}\right)\left(\frac{R}{1.5 \times 10^{11}\,\mathrm{m}}\right)^2}, \qquad (2)$$

where f_{NEO} and $f_\odot$ are the fluxes from the NEO and the Sun, respectively; Δ and R are the geocentric and heliocentric distances of the NEO at the time of the flux measurement, in meters; and p is the albedo of the NEO. For opposition surveys such as ours, R can be approximated as $\Delta + 1.5 \times 10^{11}$ meters, so to first order $R^2 \Delta^2$ is approximately Δ^4. For a given flux limit f_{NEO} and constant albedo p, diameter is therefore proportional to Δ^2. The ratio of the (geocentric) search distances for any two sizes D_a and D_b is therefore $\sqrt{D_a/D_b}$, and the ratio of searched volumes is $(D_a/D_b)^{1.5}$.

Most of our objects were detected with $\Delta < 1$ au, and all of them with $\Delta < 1.3$ au. Our detection limit of $V \sim 23$ for bodies at 1.3 au corresponds to NEOs with sizes $\sim$200 m. Thus, our survey is complete for objects larger than 200 m— that is, we would have detected every NEO larger than 200 m that appeared within our search cone—and we need only apply the volume correction described above for objects smaller than 200 m (around $H = 21$). Therefore, we set D_a above to be 200 m. We multiply our measured and debiased size distribution at every D_b smaller than 200 m by the factor $(200\,\mathrm{m}/D_b)^{1.5}$ to correct for this volume effect. This has the effect of "adding back" small ($<$200 m) NEOs that would have been in our search cone but too faint to have been detected (through being too distant).

The choice of 1.3 au as the outermost boundary of NEO space is well justified. Around 50% of our discovered NEOs have geocentric distances between 1.0 and 1.3 au, and none beyond 1.3 au. Our discovered distribution of some 70 objects indicates that the detection volume is well-sampled and extends to 1.3 au.

Finally, our survey was relatively small, covering $\sim$975 square degrees in 348 distinct pointings. We therefore

---

[11] This is similar in concept to the kind of analysis described in Schmidt (1968), though the details of the corrective approach differ.
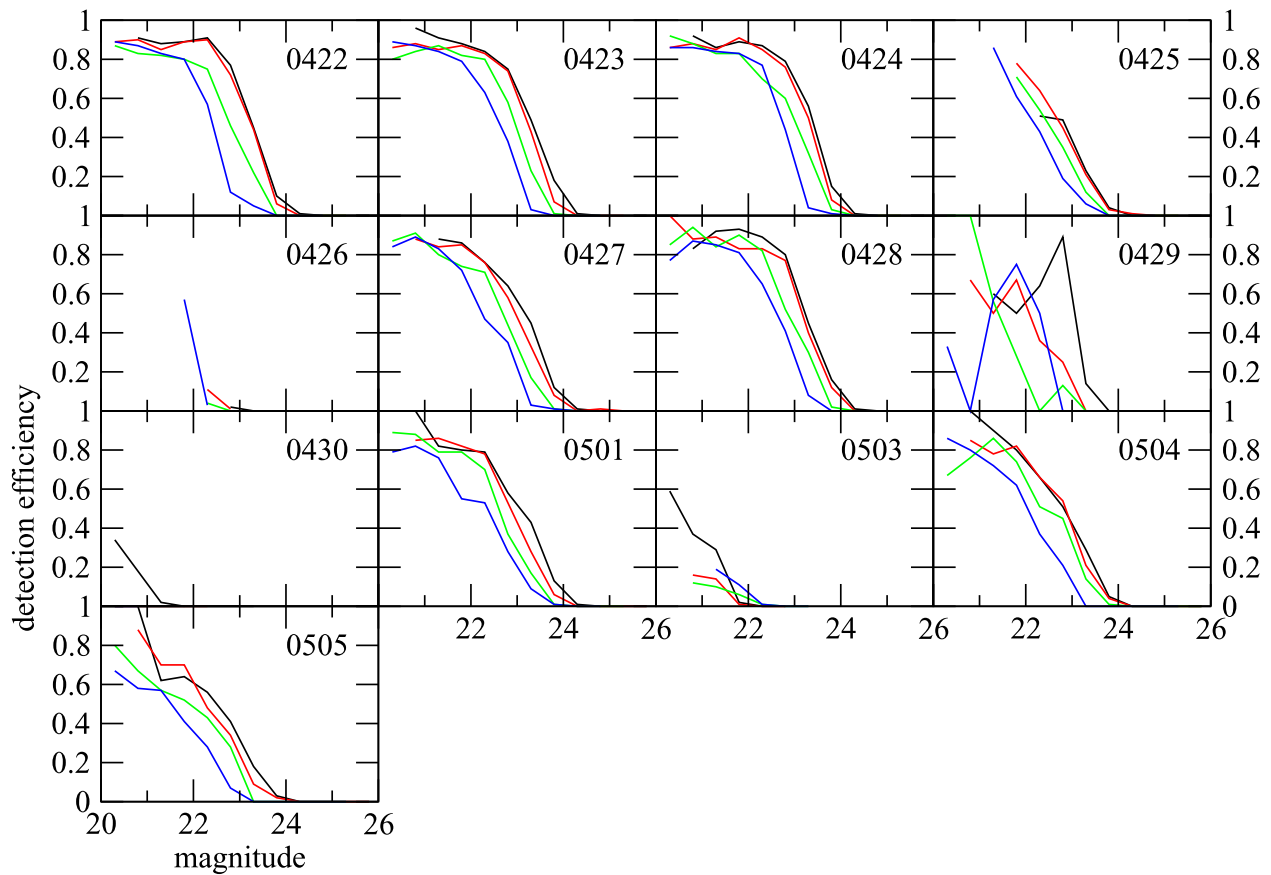
Figure 5. Nightly detection efficiencies as a function of magnitude and rate of motion. For all panels, the colors are as follows: black (60–135 arcsec hr^{-1}); red (135–210 arcsec hr^{-1}); green (210–285 arcsec hr^{-1}); and blue (285–360 arcsec hr^{-1}). There are ∼72 synthetic objects implanted within each image, resulting in more than 10,000 synthetic objects in each night. The UT date at the beginning of the night is given as MMDD. Nights with poor conditions and poor transparency are evident (0430, 0503). Night 0426 was our first experiment with implanting synthetic objects (which was not carried out on the nights in chronological order) and has fewer measured than other nights, leading to poorly defined efficiency curves. The efficiencies shown here are nightly averages. For most nights, the maximum efficiency, for slow and bright objects, is around 0.8–0.9. Typical 50% efficiency is around magnitude 23, though this depends on the rate of motion and conditions on a given night; our ability to detect fast objects is not as good as our ability to detect slower objects. In our debiasing each object is debiased according to the efficiency for the night of the observation in question and the magnitude and rate of motion of the object.
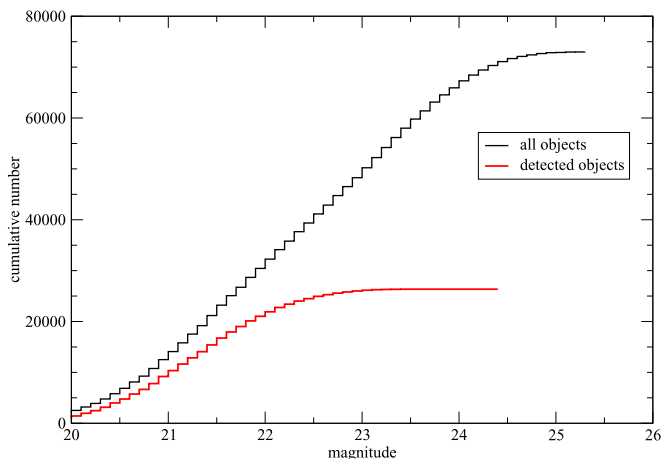
Figure 6. Cumulative number of implanted (dashed line) and detected (solid line) synthetic NEOs brighter than a given magnitude. By design, objects are implanted beyond our expected detection limit so that our detection efficiency can be measured well at the faint end. Few synthetic objects fainter than 24 were detected, as shown by the flattening of the solid line. As in Figure 3, the numbers on the vertical axis are tracklets, not point-source images. The "stair-step" pattern here simply indicates that our synthetic objects have magnitudes given only to 0.1 mag.
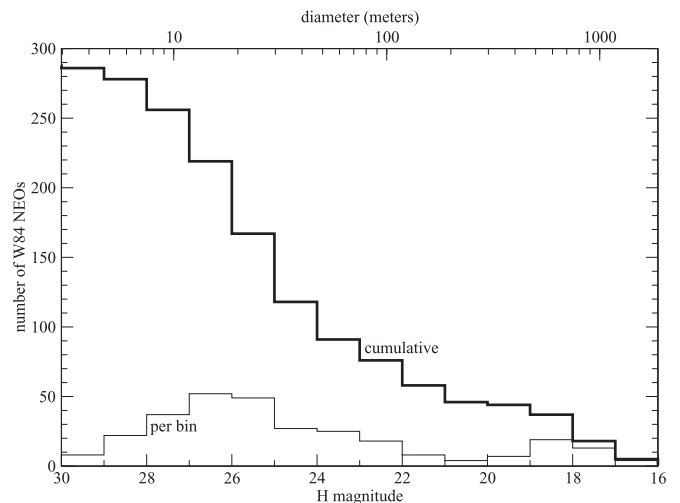
Figure 7. Histograms of H magnitudes (solar system absolute magnitudes) for all NEOs with preliminary or permanent designations that were observed in our DECam NEO survey (bottom axis). The top axis shows diameters, assuming that each object has an albedo of 0.2. The thin line shows the number of objects in each bin (0.5 mag wide), and the thick line shows the cumulative number brighter than a given H.
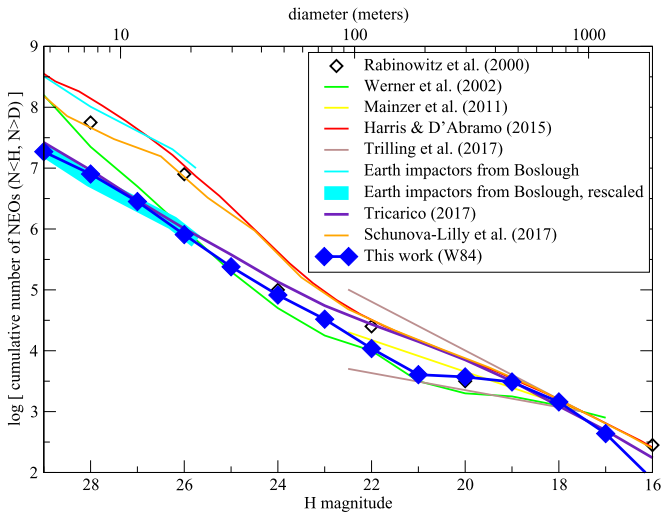
Figure 8. Cumulative debiased size distribution of NEOs. Our new result is shown as the thick blue line and data points. (Note that while our results are shown as binned data points, this binning is for representational purposes only. Each object is debiased individually according to its V magnitude, rate of motion, and distance, as described in the text.) We find around $10^{6.6}$ (or 3.5×10^6) NEOs larger than $H = 27.3$ (around 10 m), and $10^{6.9}$ (or 7.9×10^6) NEOs larger than $H = 28$ (around 7 m), assuming an albedo of 0.2 for each object. The error bars are $\sim 15\%$ for $H > 20$ and formally $\sim 5\%$ at $H > 28$; we conservatively take the overall error bar at any given size to be 10% (see the text). Our solution is normalized to have 1000 objects larger than 1 km ($H \approx 17.5$ for albedo of 0.2), which is taken from the recent NEOWISE (Mainzer et al. 2011) and Spitzer/ExploreNEOs (Trilling et al. 2017) results. Our result is in agreement with all previous estimates for $H < 22$, and for $H > 24$ it is in particularly good agreement with the recent result from Tricarico (2017). The Harris & D'Abramo (2015) and Rabinowitz et al. (2000) results have few data points for $H > 23$. The Werner et al. (2002) result assumes a size-independent impact probability that is equal to that for the largest NEOs, but our new result implies that the smallest NEOs may have a higher impact probability, requiring fewer objects to match the observed impactor population. The thin light blue line shows impactors from Boslough et al. (2015) that have been normalized using this same size-independent impact probability. The slope of the Boslough et al. (2015) result agrees extremely well with our measured size distribution, and the impact probability for small NEOs can be rederived by determining the normalization factor between the Boslough et al. (2015) bolide measurements and our results in this size range. The thick light blue line shows the Boslough et al. (2015) result, rescaled to our observations; the slopes agree very well. Our result implies a factor of 10 fewer Chelyabinsk-sized impactors than previously estimated, though with a factor of 10 greater impact probability than previously assumed.

normalize our derived size distribution to results from NEOWISE and ExploreNEOs, both of which independently derive the result that there are around 1000 NEOs larger than 1 km (Mainzer et al. 2011; Trilling et al. 2017), in agreement with an earlier estimate by Werner et al. (2002).

Our final result is shown in Figure 8. We find around $10^{6.6}$ (or 3.5×10^6) NEOs larger than $H = 27.3$ (around 10 m) and $10^{6.9}$ (or 7.9×10^6) NEOs larger than $H = 28$ (around 7 m). For the first time, the size distribution of NEOs from 1 km to 10 m has been derived from a single data set. This is significant because it bridges previous observational results that had data only at either the large or small end of this range, as discussed below.

5. Discussion

### 5.1. Objects Not Included in This Analysis

We include in this analysis only objects that have been designated and identified as NEOs by the MPC. This could introduce biases in two ways, as follows.

First, we report to the MPC only objects that have `digest2` scores of $>40\%$. We have not yet reported the many thousands of objects that we detected that have low `digest2` scores. These are objects that are likely main belt asteroids and have low probabilities of being an NEO. However, even if an object with a low `digest2` score is an NEO, the low probability indicates that it is probably moving slower than typical NEO rates, which means that it is relatively far from the Sun and Earth. In this case, the object would have to be relatively large to be bright enough to be detected by us, and would therefore have little effect on the derived size distribution of small NEOs.

In order to further understand any potential bias introduced by using `digest2`, we carried out the following experiment. We chose 10 random recently discovered objects from the MPC's list of NEOs, and for each ran only the first five measurements from the first night of observations through `digest2`. For these 10 objects, the lowest `digest2` score was 78, and seven of the objects had `digest2` NEO scores of 100 (i.e., 100% probability of being NEOs). We also chose five measurements from the discovery nights for 10 random Hungaria asteroids and 10 random Mars crossing asteroids. The Hungarias have `digest2` scores in the range of 17–66, and the Mars crossers have scores of 14–91. From this experiment, we conclude that non-NEOs can sometimes be misclassified as NEOs on the basis of their `digest2` scores (given our $\geqslant 40\%$ threshold), but no NEOs are ever misclassified as non-NEOs. We therefore do not miss any NEOs through this `digest2` filtering. Since the only objects used in this analysis are those with preliminary designations—those with orbits that are conclusively NEOs—our approach is unlikely to have either false negatives (missing objects that should be included) or false positives (including objects that should not be).

Second, objects that we observed but that never were designated are probably the faintest objects, because neither we nor any other facilities were able to recover them. Figure 9 shows that there is no correlation between H and V for $V > 20$ (a conservative limit for recovery facilities, which generally use telescopes in the 1–2 m class, though some smaller telescopes also contribute) and $H > 20$ (in other words, smaller than a few hundred meters in diameter). This lack of relationship between H and V is because there is no dependence of orbital elements on asteroid size. Therefore, there is no bias introduced in our small NEO size distribution calculation even though targets with the faintest (apparent) magnitudes may have been preferentially omitted through a recovery bias. Observed magnitude (and therefore recovery probability) is essentially independent of size for NEOs smaller than around 300 m.

Finally, there is a chance that some of the fastest moving objects were missed by our automated detection algorithms. Using this set of synthetic objects, we cannot calibrate our detection efficiency for (real) objects moving faster than 360 arcsec hr^{-1} because no synthetic objects moving faster than this rate were implanted in the data stream (Figure 4). For objects moving faster than this rate, we extrapolate our derived efficiencies (as a function of magnitude, and for the appropriate night) for the fast-moving object in question, and use these extrapolated efficiencies in our cumulative size distribution calculation. The effect of this extrapolation is small. Figure 10 shows, for our real objects, the measured rate of motion and the V and H magnitudes of those detected objects. We find that some 6.5% of real objects have rates faster than 360 arcsec hr^{-1}; for $H > 25$ (bodies smaller than 30 m), the
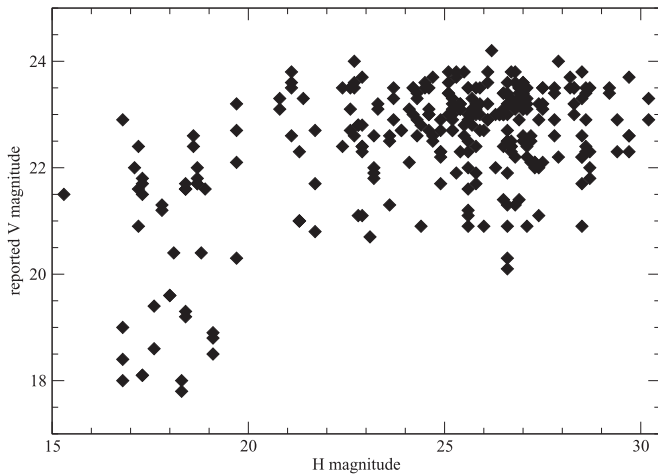
Figure 9. Reported V magnitude as a function of H magnitude for the objects used to calculate the NEO size distribution. For $V > 20$ and $H > 20$ there is no correlation between V and H, so a bias against recoveries and designations of the faintest (in V) objects does not affect the derivation of the underlying size distribution (that is, H magnitude distribution).

Figure 10. Apparent V magnitude and H magnitude as a function of rate of motion for all W84 objects reported here. Some 6.5% of objects have rates faster than 360 arcsec hr^{-1}; for $H > 25$ (bodies smaller than 30 m), the fraction is around 10%. We therefore estimate roughly that the number of small ($H > 25$) NEOs that we find could be underestimated by some 10%.

fraction is around 10%. So, while the extrapolated efficiencies are only an approximation, the relatively small uncertainty introduced affects only a small number of objects.

In conclusion, omitting some objects from this analysis for the reasons explained above likely does not introduce a significant error to our derived NEO size distribution, though we may underestimate the number of small NEOs by some 10%. We therefore conclude that the sample we consider here can be used to derive the small NEO size distribution without any large bias from reporting or recoveries.

5.2. Uncertainties

Several uncertainties remain in the size distribution estimate shown in Figure 8. One is that the photometry of our survey has uncertainties on the order of 0.1 mag, though, as described in Section 2, we formally assume photometric uncertainties of 0.2 mag. These V magnitude uncertainties transfer directly to H magnitude uncertainties.[12] Some objects may have larger uncertainties on H magnitudes if the MPC magnitudes are driven by measurements from uncalibrated surveys, so we assign a global uncertainty of 0.3 mag on all H magnitudes. (This is likely an overestimate of the uncertainties, though, since in most cases a significant fraction of the reported photometry comes from our W84 measurements, which have a relatively small uncertainty of around 0.1 mag.)

Another source of uncertainty concerns photometry of trailed sources. In our survey—as in most other NEO surveys—isophotal magnitudes are reported. For trailed objects, this typically underreports the brightness. In our survey, this affects both the real and implanted objects, so although we are internally consistent in terms of our debiasing, all fast-moving objects may actually be somewhat (perhaps a few tenths of a magnitude) brighter than reported. This error bar is on the order of the largest error described above.

Consequently, the derived size distribution shown in Figure 8 has an uncertainty in the horizontal direction on the

order of 0.3 mag. In other words, our result should be written as $10^{6.6}$ objects larger than $H = 27.3 \pm 0.3$, corresponding to diameters of 10^{+2}_{-1} m.

We have assumed that the average albedo in the NEO population is 0.2. This is the average albedo for objects smaller than 200 m as derived from NEOWISE observations (Mainzer et al. 2011). Although the NEOWISE survey is relatively insensitive to albedo, there is still a small bias against high albedo objects. Furthermore, the mean albedo for very small NEOs could be different from 0.2; if these smallest bodies have fresh surfaces (either through surface resetting due to planetary encounters, or through being collisionally young objects), then the mean albedo could be higher. Conservatively, we recalculate the above steps using mean albedos of 0.4 and, for completeness, 0.1. The result is that $H = 27.3$ corresponds to diameters of 7–14 m. This uncertainty dominates that from the previous paragraph. We conservatively express our final result as $10^{6.6}$ NEOs larger than 10 ± 4 m.

The uncertainties in our measured detection efficiencies are small because we have many thousands of objects for each night. However, there is uncertainty in our cumulative number of debiased NEOs. There are 257 NEOs with $H \leqslant 28$ in our debiased sample. Formally, Poissonian statistics implies a fidelity of around 6% on this measurement. Conservatively, we assign 10% uncertainties, which allows for other uncertainties that may be present in our result. This 10% uncertainty now also includes the possible underestimate discussed at the end of Section 5.1.

Our final result from this analysis is therefore that there are $10^{6.6} \pm 10\%$ NEOs larger than 10 ± 4 m. We note that in the context of our survey this result is still preliminary, as our 20 telescope nights from 2015 and 2016 will serve as independent measurements of the size distribution and allow us to refine our uncertainties, particularly in size regimes where we presently have a relatively small number of detections.

5.3. Comparison to Previous Estimates

There have been a number of previous estimates of the NEO size distribution, using a variety of techniques. We briefly describe previous work here, and plot their independently

---

[12] It is important to note that, in this study, we use only designated NEOs, for which orbital information is known; if we had used objects without good orbits, then the calculation of H magnitude from V magnitude would have additional uncertainties.

derived size distributions in Figure 8. All previous work agrees that there are approximately 1000 NEOs larger than 1 km, so we have normalized all the data described in this section to have 1000 NEOs at $H = 17.5$ (after Trilling et al. 2017).

Rabinowitz (1993) made an early estimate that was updated in Rabinowitz et al. (2000), in both cases using data from NEO surveys in a study that is roughly analogous to ours, though without implanting synthetic objects into the data stream. Rabinowitz et al. (2000) present results down to $H = 30$, but there are very few objects with $H > 24$ included in their solution. For $H < 24$, our results agree with those from Rabinowitz et al. (2000) very well.

More recently, Schunová-Lilly et al. (2017) have estimated the size distribution based on Pan-STARRS1 data as debiased through the (theoretical) population model of Greenstreet et al. (2012). Their population estimate is somewhat greater than ours, though they do show a change to shallower slope (and therefore a relative deficit of NEOs compared to Harris & D'Abramo 2015 for $H > 24$).

Both the Spitzer/ExploreNEOs and NEOWISE teams have made independent measurements of the size distribution of NEOs as a result of their (independent) thermal infrared surveys. NEOWISE results suggest $20{,}500 \pm 3000$ NEOs larger than 100 m (Mainzer et al. 2011); we find here around 18,000 NEOs larger than 100 m, in good agreement with the earlier result. The nominal ExploreNEOs result also suggests around 20,000 NEOs larger than 100 m, with an acceptable range of 5000–100,000 (Trilling et al. 2017); we are again in close agreement here with the previous work.

Harris et al. (2015), Boslough et al. (2015), and Harris & D'Abramo (2015) use redetection simulations of ongoing ground-based surveys to estimate completeness and therefore the underlying NEO size distribution. However, they have no simulated observations (re-detections) for objects with $H > 25$, and the completion rate is small for $H > 23$ (Boslough et al. 2015). Their estimate of the number of 10 m NEOs is therefore essentially an extrapolation from larger sizes. Our result agrees moderately well with these redetection results for $H < 23$, but the two results diverge for $H > 23$, where their number of re-detections is small. This implies that their extrapolation from larger sizes may not be appropriate.

Tricarico (2017) used a similar redetection approach and combined two decades' worth of nine different survey programs to estimate the underlying NEO population. This result is seen in Figure 8 to be in extremely close agreement with our result, especially at the smallest sizes ($H > 26$).

Werner et al. (2002) analyzed the lunar crater population to determine the size distribution of the lunar impactor population, i.e., NEOs, as averaged over the past few billion years. They estimate the NEO population down to 10 m, though with two significant caveats: (1) the average impact probability per asteroid is derived from the dynamical calculations for the $\sim$1000 largest NEOs and applied to NEOs of all sizes, and (2) there is some uncertainty whether the current NEO population is the same as the historically averaged NEO population. Our result agrees closely with Werner et al. (2002) for $H < 26$. We do not reproduce their sharp rise for $H > 26$.

Finally, Brown et al. (2013) analyzed impact data, including both the Chelyabinsk impact and various other data from the past several decades, to deduce the size distribution of Earth impactors (that is, very small NEOs). A further analysis of this impactor work is also presented in more detail in

Boslough et al. (2015). This analysis produces a size distribution of impactors covering the approximate range of 1–20 m. To convert from impactors to the entire NEO population, a scaling factor that has its origins in the calculated annualized impact rate of the 1000 largest NEOs is used (as Werner et al. 2002 did). The factor used to date places the impactor size distribution in agreement with the Harris et al. (2015) and Harris & D'Abramo (2015) NEO size distribution extrapolation in that size range.

Our measured slope from 1 to 20 m is identical to that from Brown et al. (2013) and Boslough et al. (2015), but there is an offset in the absolute number: we find $10^{6.9}$ NEOs with $H > 28$ compared to their 10^8. Their result, using their scaling from the largest NEOs, is shown as the thin cyan line in Figure 8. The thick cyan line in Figure 8 shows their impactor data normalized to our measured size distribution at $H = 26$ (around 20 m). The slopes of their impactor size distribution and our measured NEO size distribution agree extraordinarily well.

5.4. Implications of our Result

This is the first time that a single observational data set has been used to measure the size distribution from 1 km down to 10 m. Previous direct measurement work had data in either the large (>300 m) or, indirectly, the small (<20 m) regime. Very broadly, our result is in agreement with most of the previous work, but there are several aspects that warrant further exploration.

The number of $\sim$10 m sized NEOs is of keen interest because these objects impact the Earth relatively frequently and can cause severe damage (as happened in Chelyabinsk, Russia, in 2013). At this size range, our results appear to disagree with those of Rabinowitz et al. (2000) and Harris & D'Abramo (2015), but both of these have very few data points for $H > 23$. For $H < 25$, our result agrees very well with the Werner et al. (2002) result, but they report a strong upturn at $H = 26$ that is not seen in Tricarico (2017), and Schunová-Lilly et al. (2017) show a relative downturn at that same size.

The Brown et al. (2013) and Boslough et al. (2015) results for impactors in the size range of 1–20 m are significantly higher than our derived result. Werner et al. (2002), Brown et al. (2013), and Boslough et al. (2015) all have in common the assumption that the impact rate of the smallest NEOs is the same as that of the largest NEOs. If instead the impact rate of the smallest NEOs is an order of magnitude greater than that of the biggest NEOs, then the number of small NEOs implied would be reduced by that same factor. The impact rate of small NEOs could be larger than their large counterparts if the orbit distributions of those two populations differ, for example, if there exist bands of collisional debris or meteoroids in orbits similar to that of the Earth that the Earth spends significant time transiting, similar to meteor streams but with a different origin (A. Harris [DLR] 2017, personal communication). This could result, for example, from the fragmentation of medium-small NEOs into swarms of smaller boulders that pass near the Earth, such as is implied by results reported in Mommert et al. (2014a, 2014b). A very recent result (Spurný et al. 2017) suggests that one such band in which there is a relative enhancement of $\sim$10 m sized NEOs indeed may exist, and JeongAhn et al. (2016) find that the lunar cratering rate is higher for 1–10 m NEOs than for kilometer size objects. The sharp upturn in the Werner et al. (2002) distribution at $H = 26$

(Figure 8) might reflect an increasing impact probability at that size. We emphasize that the slope of the Brown et al. (2013) and Boslough et al. (2015) results for bodies 1–20 km matches our derived slope very well, implying that the discrepancy arises not from measurements of the size distribution but the normalization assumption used in their work.

We note that our data point at $H = 21$ appears depressed compared to the adjacent points and the overall implied continuum slope. This dip has been seen in other work as well (Werner et al. 2002; Harris & D'Abramo 2015; Schunová-Lilly et al. 2017). Harris & D'Abramo (2015) offer two plausible explanations. The first is that this size (around 100–200 m) corresponds to the transition from weak rubble pile asteroids at larger sizes to stronger monolithic bodies at small sizes, and that the relative deficit of bodies at this size indicates the maximally disrupted asteroid size. Their second proposed explanation is that if there is a shift in average albedo at this size (perhaps due to collisions among smaller but not larger bodies) then the conversion between H magnitude and diameter would naturally produce an apparent dip.

6. Conclusions and Future Work

We are carrying out a 30 night survey to detect NEOs with the Dark Energy Camera and the 4 m Blanco telescope at CTIO. In year one, we made 1377 measurements of 235 unique NEOs. Through implanting synthetic objects in our data stream and measuring the detection efficiency of our survey as a function of magnitude and rate of motion, we have debiased our survey. We find that there are around $10^{6.6}$ (or 3.5×10^6) NEOs larger than $H = 27.3$ (around 10 m), and $10^{6.9}$ NEOs larger than $H = 28$ (around 7 m). This population estimate is around a factor of 10 less than has been previously estimated, though in close agreement with one recent measurement and somewhat in agreement with another. Our derived NEO size distribution—the first to cover the entire range from 1 km to 10 m based on a single observational data set—matches basically all observed data for sizes larger than 100 m. In the size range of 1–20 m, our measured slope matches the bolide impactor slope quite closely, and implies that the impact probability for any given small NEOs is greater than that for a large NEO by a factor of 10 or more.

We have data from 10 survey nights in 2015 and 2016 that are not analyzed here, though all observations have already been reported to the MPC. These more recent data will be used to independently measure the size distribution and refine the error bars on the estimate presented here. We will also extend our analysis to W84 objects that were detected on only one or two nights and are therefore not designated by the MPC. This overall experiment is in some ways a pathfinder for the upcoming Large Synoptic Survey Telescope (LSST), which has NEO observations as one of its primary science drivers. LSST will have a much bigger aperture than the Blanco (8.4 m compared to 4 m), and cover far more sky than we have here (20,000 deg^2 compared to our $\sim$975 deg^2), making it the most comprehensive NEO survey ever carried out. When software tools capable of implanting and detecting synthetic objects are in place, a very high fidelity measurement of the NEO size distribution to sizes as small as 1 m will be possible.

Facility: Blanco(DECam).

Software: NOAO DECam Community Pipeline (CP) (Valdes & Gruendl 2014) with Moving Object Detection System (MODS) (Valdes 2015).

ORCID iDs

D. E. Trilling ⦿ https://orcid.org/0000-0003-4580-3790
F. Valdes ⦿ https://orcid.org/0000-0001-5567-1301
L. Allen ⦿ https://orcid.org/0000-0002-7789-5119
D. James ⦿ https://orcid.org/0000-0001-5160-4486
T. Axelrod ⦿ https://orcid.org/0000-0002-5722-7199

References

Boslough, M., Brown, P., & Harris, A. W. 2015, in Aerospace Conf. (Piscataway, NJ: IEEE), 1, http://ieeexplore.ieee.org/document/7119/

Brown, P., Assink, J. D., Astiz, L., et al. 2013, Natur, 503, 238

Christensen, E., Lister, T., Larson, S., et al. 2014, in Asteroids, Comets, Meteors —Book of Abstracts, ed. K. Muinonen et al. (Finland: Helsinki), 97

Depoy, D. L., Abbott, T., Annis, J., et al. 2008, Proc. SPIE, 7014, 70140E

Fowler, J. W., & Chillemi, J. R. 1992, IRAS Asteroid Data Processing. In The IRAS Minor Planet Survey, Tech. Rep. PL-TR-92-2049 (Hanscom AF Base, MA: Phillips Laboratory), 17

Greenstreet, S., Ngo, H., & Gladman, B. 2012, Icar, 217, 355

Harris, A. W., Boslough, M., Chapman, C. R., et al. 2015, in Asteroids IV, ed. P. Michel, F. E. DeMeo, & W. F. Bottke (Tucson, AZ: Univ. Arizona Press), 835

Harris, A. W., & D'Abramo, G. 2015, Icar, 257, 302

JeongAhn, Y., Malhotra, R., Werner, S., et al. 2016, in AAS/DPS Meeting 48 Abstract, 215.07

Magnier, E. A., Schlafly, E., Finkbeiner, D., et al. 2013, ApJS, 205, 20

Mainzer, A., Grav, T., Masiero, J., et al. 2011, ApJ, 741, 90

Mainzer, A., Bauer, J., Cutri, R. M., et al. 2014, ApJ, 792, 30

Mommert, M., Farnocchia, D., Hora, J. L., et al. 2014a, ApJL, 789, 22

Mommert, M., Hora, J. L., Farnocchia, D., et al. 2014b, ApJ, 786, 148

Monet, D. G., Levine, S. E., Canzian, B., et al. 2003, AJ, 125, 984

Rabinowitz, D., Helin, E., Lawrence, K., & Pravdo, S. 2000, Natur, 403, 165

Rabinowitz, D. L. 1993, ApJ, 407, 412

Schmidt, M. 1968, AJ, 151, 393

Schunová-Lilly, E., Jedicke, R., Vereš, P., et al. 2017, Icar, 284, 114

Spurný, P., Borovička, J., Mucke, H., & Svoreň, J. 2017, A&A, in press (arXiv:1705.08633)

Tricarico, P. 2017, Icar, 284, 416

Trilling, D., Mommert, M., Mueller, M., et al. 2017, AJ, submitted

Valdes, F. 2015, in ASP Conf. 495, Astronomical Data Analysis Software an Systems XXIV, ed. A. R. Taylor & E. Rosolowsky (San Francisco, CA: ASP), 95

Valdes, F., & Gruendl, R. 2014, in ASP Conf. 485, Astronomical Data Analysis Software and Systems XXIII., ed. N. Manset & P. Forshay (San Francisco, CA: ASP), 379

Wainscoat, R., Veres, P., Bolin, B., et al. 2014, in Asteroids, Comets, Meteors —Book of Abstracts, ed. K. Muinonen et al. (Finland: Helsinki), 574

Werner, S. C., Harris, A. W., Neukum, G., & Ivanov, B. A. 2002, Icar, 156, 287